BRIAN J. ANDERSON

ULTRA-LOW-FREQUENCY MAGNETIC PULSATIONS IN THE EARTH'S MAGNETOSPHERE

Regular magnetic field oscillations in the Earth's magnetosphere occur continuously and are one way solar wind energy is deposited in the ionosphere. Recent determinations of the occurrence distributions of these oscillations imply that pulsations are coupled to solar wind energy by several mechanisms and may be a more significant energy source for the sub-auroral ionosphere than previously thought.

INTRODUCTION

Although we usually regard the magnetic field measured on the Earth as constant, many geomagnetic processes introduce perturbations in the field. Auroral activity and the associated ionospheric current systems produce significant magnetic disturbances often as large as 1000 nanoteslas (nT), or about one-sixtieth of the Earth's field strength at the ground.* Other fluctuations also occur; although these are smaller (typically ≈ 10 nT), they are distinguished by their remarkable regularity. These regular fluctuations are called geomagnetic pulsations and appear as nearly sinusoidal waveforms in ground-station magnetometer records with periods ranging from 0.5 s to 10 min.[1]

As with the auroral currents, geomagnetic pulsations originate in magnetospheric processes. They occur at all local times and under a variety of circumstances. Spacecraft observations have shown that these pulsations, despite their small amplitude on the ground, have amplitudes in space relative to the local magnetic field of 5% to 10% and occasionally much larger, up to about 50%. By studying geomagnetic pulsations, a detailed comparison can be made between plasma physics theory and observations in ways not possible in laboratory experiments. In addition, geomagnetic pulsations play a role in magnetospheric dynamics and energy transport, and their study forms an integral part of increasing our understanding of the magnetosphere.

Importance of Spacecraft Observations

Space-based instrumentation has provided the greatest insight into pulsations. By measuring the *in situ* magnetic field perturbations, the polarization characteristics and frequency structure of pulsations have been determined unambiguously. Electric field and particle instruments have also been used to test pulsation theories in ways not possible with ground observations.[2,3] Multi-spacecraft and satellite–ground correlation studies have been performed to study the spatial distribution and propagation characteristics of pulsations.[4-6] As a result of the extensive analysis of satellite data, the primary pulsation mechanisms have been identified.

*The nominal value of the Earth's field near the poles is 60,000 nT; 1 nT = 10^{-5} gauss.

The vast majority of satellite data comes from geostationary or near-geostationary spacecraft, so that the region of space most heavily sampled in the magnetosphere corresponds to a narrow annulus in the equatorial plane. Because of the small volume that spacecraft have sampled to date, it is not well known to what extent pulsations near geosynchronous orbit are representative of pulsations occurring in other regions of the magnetosphere. Hence, although various pulsation mechanisms have been identified, and considerable progress in confirming theories of magnetic pulsations has been made, numerous questions about the relationships between pulsations and magnetospheric dynamics and energy transport remain to be adequately addressed.

Unique Role of the AMPTE/CCE Satellite

The Active Magnetospheric Particle Tracer Explorers/Charge Composition Explorer (AMPTE/CCE) satellite has several features that make it useful for pulsation studies. A primary factor is the satellite's elliptical orbit with a maximum altitude of 7.8 R_E (8.8 R_E apogee, 1 R_E = 6380 km, where R_E denotes Earth radii) and low geographic inclination (5°), which provide $\pm 16°$ magnetic latitude (MLAT) coverage.[7] Equally important is the quantity of data available. The satellite functioned from August 1984 to January 1989, during which time excellent data coverage (90%) was achieved. The CCE data therefore provide extensive sampling of a sizable volume of the magnetosphere. In addition, the Magnetic Fields Experiment on the CCE spacecraft, performed by APL, was a sophisticated design with seven automatically switchable ranges providing 0.01% resolution of fields from 16 to 65,535 nT full scale. The sampling rate was 8.06 vector samples per second, so that the maximum detectable frequency was 4.03 Hz, providing excellent frequency coverage.[8] Fortuitously, computational power has recently become more economical, allowing sophisticated data processing to be performed on a routine basis that was not possible previously. This combination of factors—satellite orbit and data coverage, sophisticated magnetic field instrumentation, and the development of relatively inexpensive computational resources—allows a significant advance in magnetic pulsation studies based on the AMPTE/CCE data set.

The first analysis of AMPTE/CCE magnetic field data specifically directed to pulsation studies was undertaken by Mark J. Engebretson of Augsburg College in Minneapolis, Minnesota, in collaboration with Thomas Potemra and Lawrence Zanetti, both of APL.[9] The first results clearly showed that the AMPTE/CCE data would make a significant contribution, and the studies done subsequently by Engebretson and also by Kazue Takahashi of APL showed that a variety of pulsations was observed by AMPTE/CCE.[10,11] Subsequent statistical studies conducted by the author in collaboration with Engebretson, Potemra, Zanetti, and Takahashi were done to determine the occurrence distributions of pulsations in the magnetosphere. The results of these studies provide considerable insight into the role of pulsations in magnetospheric processes and will be discussed later after introducing the physics of the relevant wave phenomena in the magnetosphere.

WAVES IN THE MAGNETOSPHERE

Before discussing the CCE observations, it is useful to sketch the characteristics of the plasma medium that determine what waves are supported in the magnetosphere. The waves occurring in the 0.5-s to 10-min period range are of two basic types: (1) standing wave resonances and (2) plasma instabilities. Magnetospheric standing waves are analogous to standing waves on a string (shear waves) or in an organ pipe (longitudinal sound waves) and result from the interplay of the geometry of the Earth's magnetic field and waves supported by the plasma medium. The standing waves observed are those whose frequency and spatial structure most nearly match those of the driving source(s). Plasma instabilities result from the interaction of charged particle distributions with electromagnetic fields, and their occurrence is determined principally by the characteristics of the magnetospheric particle distributions.

The Magnetospheric Medium

An appreciation of the variety of waves supported in the Earth's magnetosphere is afforded by a comparison with sound waves. In air, the only wave mode supported consists of disturbances of alternating regions of compression and rarefaction. The disturbances propagate in the direction of the pressure variations with a uniform speed called the sound speed, v_s. The wavelength λ and frequency f of the waves are related by the simple expression $\lambda f = v_s$. The notation $\omega = kv_s$ is commonly used, where $\omega = 2\pi f$ and $k = 2\pi/\lambda$. On the microscopic scale, the forces between air molecules are transmitted entirely by collisions; between collisions, the molecules travel in straight-line trajectories.

In a magnetized plasma, the situation is vastly more complex. Magnetospheric plasma is a fully ionized gas composed of electrons and protons with admixtures of He^+ ($\approx 5\%$–10%), O^+(1%–2%), and He^{2+} ($\leq 1\%$). The density is exceedingly low, about 10 to 1000 particles/cm^3, compared with 3×10^{19} particles/cm^3 in air at room temperature, so that plasma particles move essentially without collisions. (A collision in a plasma is different than in air because it is caused by long-range coulomb forces that are screened with a length scale called the Debye length.) Even though the particles do not collide, their motions are complex and are not straight-line trajectories. Because the particles have a charge q, they experience a force $\mathbf{F} = q(\mathbf{E} + \mathbf{v} \times \mathbf{B})$, called the Lorentz force, which is due to electric and magnetic fields, $\mathbf{E}$ and $\mathbf{B}$, respectively. Via this force, the magnetic field constrains the particles to move along the magnetic field lines and to gyrate around the field lines, electrons in the right-hand sense and ions in the left-hand sense. This perpendicular circular motion occurs with the angular frequency $\Omega_c = qB/m$ and a radius $r_c = v_\perp m/qB$, where m is the particle mass and $v_\perp$ is its velocity perpendicular to $\mathbf{B}$. Because of the particle's charge, the circular motion produces a magnetic moment $\mu = -mv_\perp^2\mathbf{B}/2B^2$. Since μ is directed opposite to $\mathbf{B}$, the plasma is a diamagnetic medium.

Influence of the Plasma

The plasma also exhibits collective behavior because the ions and electrons not only respond to electric and magnetic fields, but they also participate in their generation. Minute charge imbalances generate electric fields and relative motion of the electrons, and ions generate currents and hence magnetic fields. The particles, in turn, react to these fields according to the Lorentz force, so that the large-scale fields feed back on the motions that caused them. This interplay of particle motions and electromagnetic fields is given analytically by Maxwell's equations: $\nabla \cdot \mathbf{E} = \rho$, $\nabla \cdot \mathbf{B} = 0$, $\nabla \times \mathbf{E} = -\partial\mathbf{B}/\partial t$, and $\nabla \times \mathbf{B} = \mu_0(\mathbf{J} + \epsilon_0 \partial\mathbf{E}/\partial t)$, where ρ is the charge density; t is time; $\mathbf{J}$ is the current density; and μ_0 and ϵ_0 are the permeability and permittivity of free space, respectively.

In the treatment of linear plasma waves, the field perturbations are transformed by letting the field quantities vary as $\exp[i(\mathbf{k} \cdot \mathbf{r} - \omega t)]$, where $\mathbf{k}$ is the wave vector, $\mathbf{r}$ is the position vector, ω is the angular frequency, and $i = \sqrt{-1}$, to solve the problem for particular $\mathbf{k}$ and ω. With this transform and by using the Lorentz force, the particle motions can be computed, and the plasma's response to the electromagnetic field can be written in terms of a conductivity matrix σ, so that the current density $\mathbf{J}$ is given by $\mathbf{J} = \sigma \cdot \mathbf{E}$. By using Maxwell's equations, an expression involving only the electric field can be obtained of the form $\mathbf{M} \cdot \mathbf{E} = 0$, where $\mathbf{M}$ is a matrix; the equation only has solutions if the determinant of $\mathbf{M}$ vanishes. This condition yields the plasma dispersion relation $D(\mathbf{k}, \omega) = 0$, and solutions of this relation for which $\mathrm{Re}(\mathbf{k}) \neq 0$ are supported as waves in the plasma. Furthermore, those solutions with $\mathrm{Im}(\omega) < 0$ are damped, whereas those with $\mathrm{Im}(\omega) > 0$ grow exponentially and are unstable. Since $D(\mathbf{k}, \omega)$ is a complicated function, characterizing its solutions involves appreciable effort but shows that a wide array of wave phenomena can occur.[12]

Influence of the Ambient Magnetic Field

A magnetized plasma is not isotropic but exhibits a distinction between motions parallel and perpendicular to $\mathbf{B}$. This anisotropy appears in the expression for the plas-

ma pressure. The total plasma pressure is given by $P = P_{part} + B^2/2\mu_0$, where the magnetic contribution to the pressure is the magnetic energy density, just as P_{part} is the kinetic energy density of the particles. In addition, it is useful to consider the particle pressure as derived from two contributions, $P_{part} = P_\perp + P_\parallel$, where $P_\perp$ is the pressure due to motions perpendicular to **B**, and $P_\parallel$ is that due to motions parallel to **B**. Because the particle gyromotions lead to diamagnetic moments, as discussed earlier, the perpendicular pressure leads to a magnetic moment per unit volume of $\mathbf{m} = -P_\perp \mathbf{B}/B^2$.

The analog of sound waves in air occurs, but because the magnetic field also contributes to the total pressure, "sound-like" waves propagating parallel and perpendicular to the field are different. Compressional waves traveling along the magnetic field are governed only by P_{part}, but compressions traveling perpendicular to **B** are affected by both P_{part} and the magnetic pressure, and the wave speed is either raised or lowered according to whether the magnetic and particle pressure fluctuations are in phase (fast mode) or out of phase (slow mode).

In addition to longitudinal sound-like waves, the magnetic field introduces a new class of transverse waves called shear Alfvén waves. These waves occur because the magnetic field provides a tension per unit area, B^2/μ_0, which acts to restore perturbations in the field to the equilibrium configuration. This phenomenon is analogous to the way waves are supported on a string. For a string under a tension T with a linear mass density ρ_l, waves travel at a speed $V = \sqrt{(T/\rho_l)}$. In a magnetized plasma, B^2/μ_0 provides the tension, and the plasma provides the mass density ρ_m, so that the speed of shear Alfvén waves is $V_A = \sqrt{(B^2/\mu_0\rho_m)}$. It turns out that shear Alfvén waves are guided along the magnetic field, so that the waves follow the bends in the field.

Particle Motions: Gyration, Bounce, and Drift

Because of the highly structured nature of particle motions, the particles introduce waves and interactions with waves that have no corollary with sound waves. Since the ions gyrate about the magnetic field in a left-hand sense, this motion leads to so-called ion cyclotron wave modes, which are left-hand waves. The presence of several ionic species with different mass-to-charge ratios—H^+ (1 amu/e), He^+ (4 amu/e), and O^+ (16 amu/e)—implies the existence of a set of ion cyclotron frequencies, so that the different species interact differently with electromagnetic waves if the frequency is between cyclotron frequencies. Hence, several different waves associated with particle gyromotions appear in a multicomponent plasma.[13] It turns out that ion cyclotron waves occur principally in the vicinity of the He^+ gyrofrequency, which varies from 4.4 Hz near 3 R_E to 0.16 Hz at 9 R_E in the equatorial plane of the Earth's field. The CCE magnetic fields instrument, which has a Nyquist frequency (upper frequency limit) of 4.03 Hz, is therefore well suited to detecting the waves in this region. Electrons gyrate in a right-hand sense and are associated with right-hand waves. Because the electron mass is a factor of 1830 less than the mass of H^+, however, the electron cyclotron frequency ranges from 1 to 10 kHz, far above the sampling rate of the CCE magnetic fields instrument.

In addition to their gyromotion, particles bounce back and forth between the Northern and Southern hemispheres in the dipole field of the Earth. Those particles whose velocities at the magnetic equator are most aligned with the magnetic field travel farthest along the field line and are reflected at the lowest altitudes. Bounce periods for typical magnetospheric protons range from 50 to 150 s. This motion is of interest here because of the potential for resonance between particle bounce motions and magnetic field-line resonance frequencies.

As particles bounce between the Northern and Southern hemispheres, they also drift azimuthally in the dipole field because of the combined effects of field-line curvature and radial gradient in field intensity. Ions drift westward and electrons drift eastward. For typical particle energies (<200 keV), the period for a complete drift around the Earth is much longer than 10 min, so the frequency of this motion is not of interest here. What is important is that the particles drift around the Earth, ions one way and electrons the other.

Large-scale electric fields also lead to particle drift, with the difference that electrons and ions drift in the same sense. Particles respond to an imposed electric field **E** by drifting with a drift velocity $\mathbf{V}_{DE} = \mathbf{E} \times \mathbf{B}/B^2$, that is, perpendicular to both **E** and **B**. This electric field drift will be important in a later discussion of drift waves. In addition, the solar wind flow past the magnetosphere creates an electric field throughout the magnetosphere that is generally directed from dawn to dusk. Because the magnetic field in the equatorial plane is northward, this dawn-to-dusk electric field causes plasma to drift sunward. This sunward motion of plasma plays an important role in transporting energetic ions from the tail of the magnetosphere toward the inner magnetosphere, where they excite magnetic pulsations.

Having briefly discussed the medium in which pulsations occur, we can now consider the manifestations of field-line resonances and waves arising from plasma instabilities in the magnetosphere.

FIELD-LINE RESONANCES

The dipolar field lines of the Earth's field can be regarded as anchored in the northern and southern ionospheres, and shear Alfvén waves guided along the field direction will be reflected by the highly conductive ionosphere so that the field lines actually constitute a linear resonance cavity. Figure 1 shows two examples of field-line perturbations associated with different field-line resonance modes. In the figure, displaced field lines are shown relative to their equilibrium positions. The coordinate system indicated by the unit vectors is the dipole system discussed later. The azimuthal perturbation, Figure 1A, consists of a side-to-side motion of the field line, and the outward perturbation, Figure 1B, consists of stretching (compression one-half cycle later) of the field line.

The String Analogy

As with waves on a string, the field-line resonances are standing waves, and each field line admits a harmonic ser-

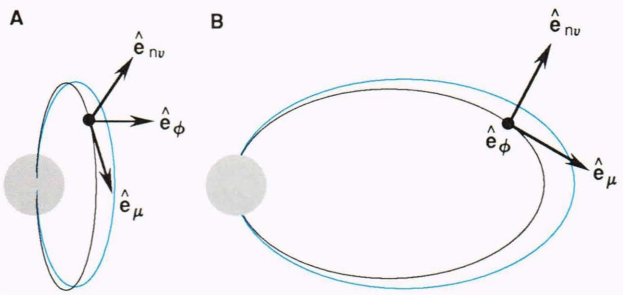

Figure 1. Field-line displacements. **A.** Fundamental toroidal (azimuthal) field-line resonances. **B.** Poloidal (outward) field-line resonances. The dipole coordinate system—ν, μ, ϕ—used to analyze the resonances analytically is also shown. Displacements correspond to standing waves along the field lines.

ies of resonant frequencies corresponding to successively shorter wavelengths established between its end points. For a string of length l and uniform wave velocity V, the resonant wavelengths are those that fit in l with a half integral number of wavelengths. The nth harmonic has a wavelength $l_n = 2l/n$ and a frequency $f_n = nV/2l$. More generally, the wave equation for transverse waves on a string is $V(x)^2\partial^2\psi/\partial x^2 = \partial^2\psi/\partial t^2$, where V is a function of longitudinal distance x, and ψ is the transverse displacement of the string from its equilibrium position. The solutions are determined by solving this equation subject to the boundary conditions $\psi(0) = \psi(l) = 0$.

Qualitatively, field-line resonances are essentially the same.[14] Figure 2 shows schematic representations of the field-line displacement ξ and magnetic field perturbation for the first three harmonic resonances. In the figure, the dipole geometry is replaced by a linear model in which the field line is anchored in the northern and southern ionospheres, represented by the shaded regions. The field-line displacements are shown at times of largest amplitude when the field line is at rest instantaneously. The field-line displacement is analogous to the displacement of a vibrating string, but it is not the magnetic field perturbation. Rather, the perturbation $\delta\mathbf{B}$ is given by the derivative of the vector displacement ξ, $\delta\mathbf{B} = B_0\partial\xi/\partial s$, where B_0 is the unperturbed field magnitude and s is distance along the field line. The perturbation has nodes where the vector displacement ξ is a local maximum. Because the magnetic field oscillates, the standing wave is associated with a motional electric field given by $\mathbf{E} = -\partial\xi/\partial t \times \mathbf{B}_0$. Note that $\mathbf{E}$ and $\delta\mathbf{B}$ are perpendicular and 90° out of phase. In addition, the number of nodes in $\delta\mathbf{B}$ equals the harmonic number, and odd harmonics have nodes at the equator, whereas even harmonics have anti-nodes at the equator. In addition, $\mathbf{E}$ has anti-nodes where $\delta\mathbf{B}$ has nodes and vice versa. Because the field-line displacement of odd harmonics is symmetric about the equator, the odd harmonics are called symmetric modes, whereas the even harmonics are antisymmetric in the field-line displacement. This distinction is important because sources that displace the field at the equator will primarily excite the symmetric, odd harmonic modes. Both the latitudinal structure and relationship between $\mathbf{E}$ and $\delta\mathbf{B}$ have been confirmed observationally.[2]

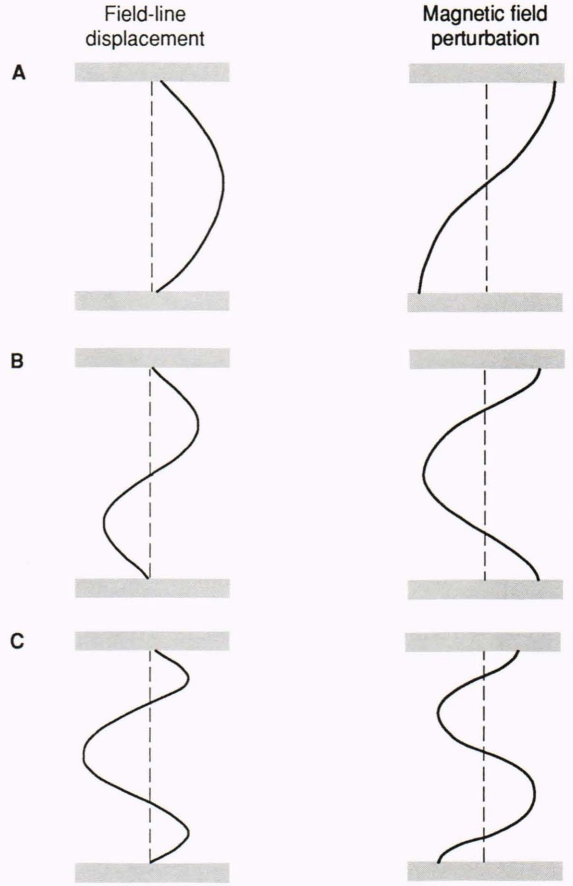

Figure 2. One-dimensional model of field-line resonances. The northern and southern ionospheric boundaries are represented by the shaded regions. **A.** Harmonic number (n) = 1. **B.** n = 2. **C.** n = 3.

Quantitative Analysis for a Dipole Field

A quantitative analysis of field-line resonances is more complicated than that for waves on a string because (1) the wave speed varies greatly along the field line, and (2) the problem is three-dimensional in a non-Cartesian geometry. The wave equation is obtained from ideal magnetohydrodynamics, in which the plasma is treated as an infinitely conductive fluid, and only frequencies much lower than the lowest ion cyclotron frequency are considered. The result for the electric field is $\partial^2\mathbf{E}/\partial t^2 = 1/(\mu_0\rho_m)\,\mathbf{B}_0 \times \mathbf{B}_0 \times \nabla \times \nabla \times \mathbf{E}$, where ρ_m is the plasma mass density.[15] Recalling that $V_A = B_0/\sqrt{(\mu_0\rho_m)}$, we see that this equation is completely analogous to the wave equation for a string, except that the cross product and curl have replaced scalar multiplication and differentiation, respectively. The dipole coordinates—ν, μ, and ϕ—shown in Figure 1, are introduced to treat the problem: $\hat{\mathbf{e}}_\nu$ is perpendicular to the field line and pointed outward, $\hat{\mathbf{e}}_\mu$ is directed along the field line, and $\hat{\mathbf{e}}_\phi$ is in the azimuthal direction. If the standing wave is purely transverse, that is, $\delta B_\mu = 0$, the wave equation separates into two uncoupled equations, one for E_ϕ, δB_ν, and one for E_ν, δB_ϕ. The mode with $dB_\phi \neq 0$ is the toroidal mode, where the magnetic field perturbation is purely azimuthal; the mode with $dB_\nu \neq 0$

is the poloidal mode, where the magnetic field perturbation is purely outward, that is, radial at the equator. Referring to Figure 1, we see that part A corresponds to $\delta\mathbf{B} = \delta B_\phi \hat{\mathbf{e}}_\phi$ (the toroidal mode), and part B corresponds to $\delta\mathbf{B} = \delta B_\mu \hat{\mathbf{e}}_\mu$ (the poloidal mode).

Consideration of Figure 1 suggests that if a single field line were displaced, it would necessarily crowd neighboring field lines. This crowding corresponds to a compressional perturbation, and hence the assumption that $\delta B_\mu = 0$ is not strictly valid. The complete three-dimensional wave problem in a dipole geometry has yet to be solved analytically, but numerical simulations[16] and analytical treatments[17,18] have shown that despite the violation of this assumption, the basic ideas are sound, and the simple theory provides an excellent approximation. In addition, toroidal and poloidal resonances have been observed to occur and to be only weakly coupled, and their periods have been found to be consistent with this simple theory.

Determining resonance periods from the wave equation requires assuming a function for ρ_m. Good agreement with measured pulsation frequencies is provided by a power law with radial distance $\rho_m = \rho_{m0}(r/r_0)^{-q}$ with $q \approx 4$, where ρ_{m0} is the mass density at the equatorial crossing distance of the field line, r_0. Figure 3 shows the toroidal fundamental mode resonance period for $r_0 = 5$ to 10 R_E. The period varies with r_0 approximately as r_0^2; the radial variation of the period is one of the signatures used to identify pulsations as field-line resonances. The ratios of the toroidal fundamental mode period to other toroidal harmonics and to the poloidal mode periods are independent of distance and are given in Table 1. With the exception of the fundamental mode, the toroidal and poloidal mode periods are essentially the same. For a simple harmonic series, the periods T_1 and T_2 of harmonics n_1 and n_2 are related by $T_1/T_2 = n_2/n_1$. With the exception of the fundamental mode, the resonance periods occur in a nearly simple harmonic series.

Field-Line Resonances in the Magnetosphere

Because of field-line resonances, the magnetosphere contains a continuous set of resonators, each of which can oscillate at several harmonics in two approximately decoupled modes, poloidal and toroidal. In principle, the frequency that could be excited has no upper limit, but resonance frequencies greater than 0.1 Hz (10-s period) are not observed, presumably because the driving source for higher frequencies is not structured properly in space to drive the resonance coherently over the length of the field lines. By measuring the polarization, frequency structure, and distribution with magnetic latitude, the mode and harmonic of field-line resonances observed in space can be determined. This information provides important clues about the energy source coupling to the resonance because the energy source must match the spatial structure of the resonance.

Fundamental Mode Toroidal Resonances

An example of a toroidal fundamental mode resonance is shown in Figure 4. The spectrogram shows wave power

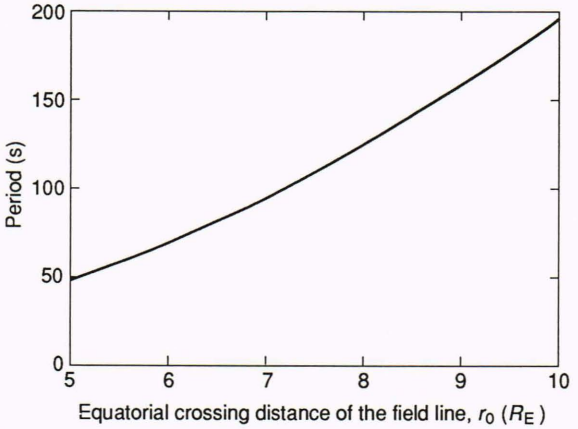

Figure 3. Period of the fundamental toroidal mode field-line resonance versus the equatorial crossing distance of the field line, r_0. An equatorial mass density $\rho_{m0} = 50(5/r_0)^4$ (amu/cm^3) was assumed. The ratios of poloidal modes and toroidal mode harmonics are independent of r_0 (see Table 1).

Table 1. Ratios between various toroidal mode periods and poloidal mode periods.

n	T_1/T_n	P_n/T_n	T_2/T_n	$n/2$
1	1.00	1.37	0.44	0.5
2	2.28	1.01	1.00	1.0
3	3.56	1.00	1.57	1.5
4	4.84	1.00	2.12	2.0
5	6.12	1.00	2.68	2.5
6	7.39	1.00	3.24	3.0

Note: n is the harmonic number, T_n is the toroidal mode for the nth harmonic number, and P_n is the poloidal mode for the nth harmonic number.

versus frequency for one orbit of the AMPTE/CCE satellite. The coordinate system is a spherical system with B_R radially outward, B_E eastward, and B_N northward, tangent to the sphere. Component B_E is in the $\hat{\mathbf{e}}_\phi$ direction, and because the spacecraft is near the equatorial plane, B_N is close to the $\hat{\mathbf{e}}_\mu$ direction and B_R is close to $\hat{\mathbf{e}}_\nu$. The magnetic coordinates of the spacecraft are listed under the spectrogram (L is the equatorial crossing distance of the field line passing through the spacecraft in units of R_E, and MLT is magnetic local time). The presence of a toroidal, nearly monochromatic wave is evident from 2300 to 0700 UT. The waveform shows the sinusoidal nature of the wave. Later in the orbit, especially after 0700 UT, higher harmonics are observed, again in the toroidal mode. The period of the fundamental mode is about 200 s (5 mHz), and the harmonics appear in the period range from 20 to 50 s (50 to 20 mHz), in good agreement with theory.

In studies carried out by the author in collaboration with Engebretson, Potemra, Zanetti, and Shawn Rounds, the occurrence distribution of pulsations in the CCE data set was evaluated by using fifteen months of data.[19] The latitude and L/MLT occurrence frequency distributions were

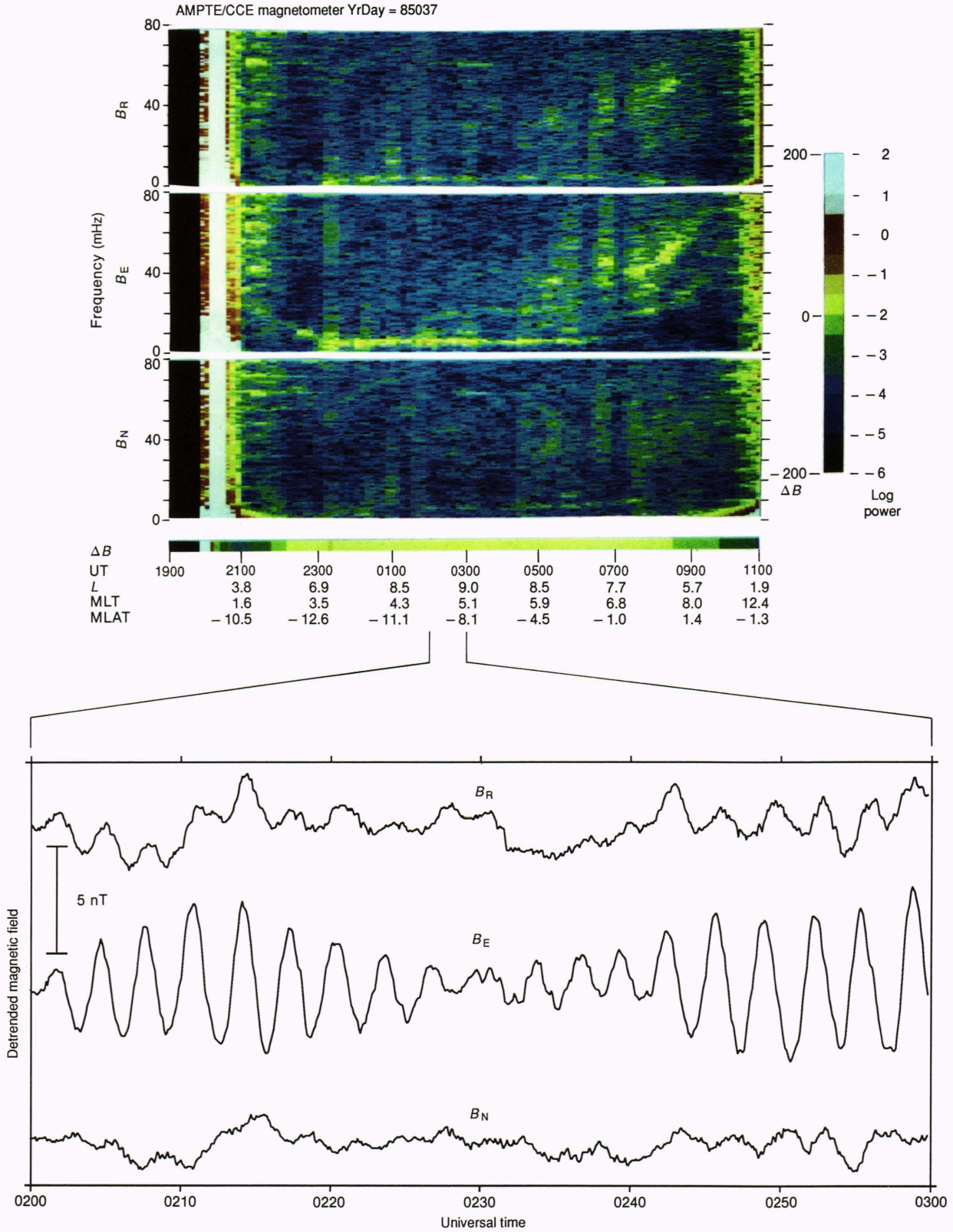

Figure 4. Example of the toroidal fundamental mode field-line resonance observed by the AMPTE/CCE Magnetic Fields Experiment. The spectrograms show wave power as a function of frequency versus universal time (UT) for one satellite orbit. The magnetic field components are B_R, radially outward; B_E, azimuthal; and B_N northward and approximately along the field direction. Spacecraft coordinates are indicated below the spectrogram: L is the equatorial crossing distance of the field line passing through the spacecraft in units of R_E, MLT is magnetic local time, and MLAT is magnetic latitude. The one-hour segment of detrended data illustrates the sinusoidal nature of the wave and the dominance of the azimuthal component.

determined by taking the ratio of the elapsed occurrence time of particular pulsation types to the total observation time in each latitude and L/MLT bin. The distributions for fundamental toroidal resonances are shown in Figure 5. The latitude distribution clearly shows a node at 0° MLAT with monotonically rising occurrence frequency, reflecting the nodal structure in the magnetic perturbation of the fundamental mode. The equatorial distribution shows a clear maximum at 0500 to 0700 MLT, L = 8–9. The dawn/dusk asymmetry is remarkably strong, although several other pulsations often occur at dusk (as discussed later); thus, it is difficult to conclude that the asymmetry of occurrence reflects a correspondingly strong asymmetry in resonance excitation. Interference from other pulsations does not occur on the dayside (0900–1500 MLT) or the nightside (2100–0300 MLT), so the preference for excitation at the flank does reflect the localization of the energy source. The decrease in occurrence frequency with L may be due to the low frequency of the source as follows: because the resonance frequencies increase with decreasing radial distance, the frequency-matching condition will not be met on inner field lines if the driving source frequency is sufficiently low, and hence resonance will not occur.

A primary candidate for the source of these waves is the Kelvin–Helmholtz, or wind-on-water, instability excited by sheared plasma flows occurring near or just inside the magnetopause at the flanks. Theoretical studies have shown that the flanks are an appropriate site for generating long wavelength ($\approx 10\ R_E$) surface waves, whereas near noon, the flow speeds are too low to drive the instability.[20]

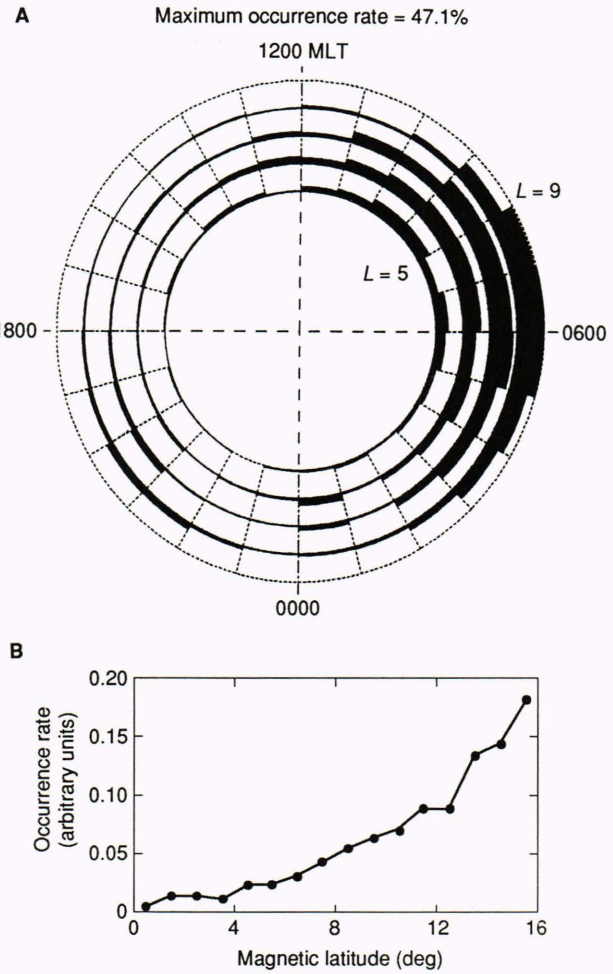

Figure 5. Occurrence distributions of fundamental toroidal mode field-line resonances in the Earth's magnetosphere. **A.** Equatorial occurrence distribution. **B.** Latitude occurrence distribution. The equatorial occurrence frequencies are a percent of total observation time, and the latitude occurrence frequency scale is arbitrary. MLT is magnetic local time, and L is the equatorial crossing distance of the field line passing through the spacecraft in units of R_E.

Toroidal Harmonic Series

An example of a second population of field-line resonances is shown in Figure 6. From 0530 to 1000 UT and again from 1500 to 1800 UT, toroidal harmonic resonances occur over the frequency range from 15 to 40 mHz. The waveform shows small-amplitude sinusoidal pulsations, but it is difficult to discern the harmonic structure from the line plot, illustrating the advantage of the spectrogram display. The latitude and L/MLT distributions of these harmonic resonances are shown in Figure 7. The latitude distribution is fairly uniform with only a shallow minimum at 0° MLAT, indicating the presence of both even and odd harmonics. The L/MLT distribution shows that the waves are a dayside phenomenon and occur with roughly equal probability over a wide L range. This distribution implies that the energy source is on the dayside and that inward propagation of energy is relatively efficient. Other work has shown that these harmonic pulsations are correlated with the alignment of the interplanetary magnetic field with the Earth–Sun line;[21,22] thus, the excitation of these waves is caused directly by the solar wind/magnetosphere interaction.

Poloidal Mode Oscillations

An example of the third class of field-line resonance pulsations identified in the CCE data is shown in Figure 8. The pulsations occur from 2200 to 0200 UT and again from 0500 to 0630 UT and are predominantly radial, indicating a poloidal mode. The latitude and L/MLT distributions (Fig. 9) show that the occurrence probability maximizes at the equator, implying an even harmonic. The wave period is in the range from 50 to 100 s, also suggesting that it is probably a second harmonic (cf. Fig. 3). The L/MLT distribution is markedly different from the fundamental and harmonic mode field-line resonances. The occurrence pattern is a band that shifts from $L > 7$ at night to $L < 7$ on the dayside, with an absence of waves in the morning. It has a significant population of nightside events, a condition that does not suggest a direct energy source in the solar wind/magnetosphere interaction. That the waves are even harmonics implies that the energy source acts asymmetrically about the equator. Researchers have suggested previously, on the basis of these properties, that poloidal resonances are second harmonics in bounce resonance with energetic ions,[23] and Takahashi et al.[11] showed directly in one case study with simultaneous

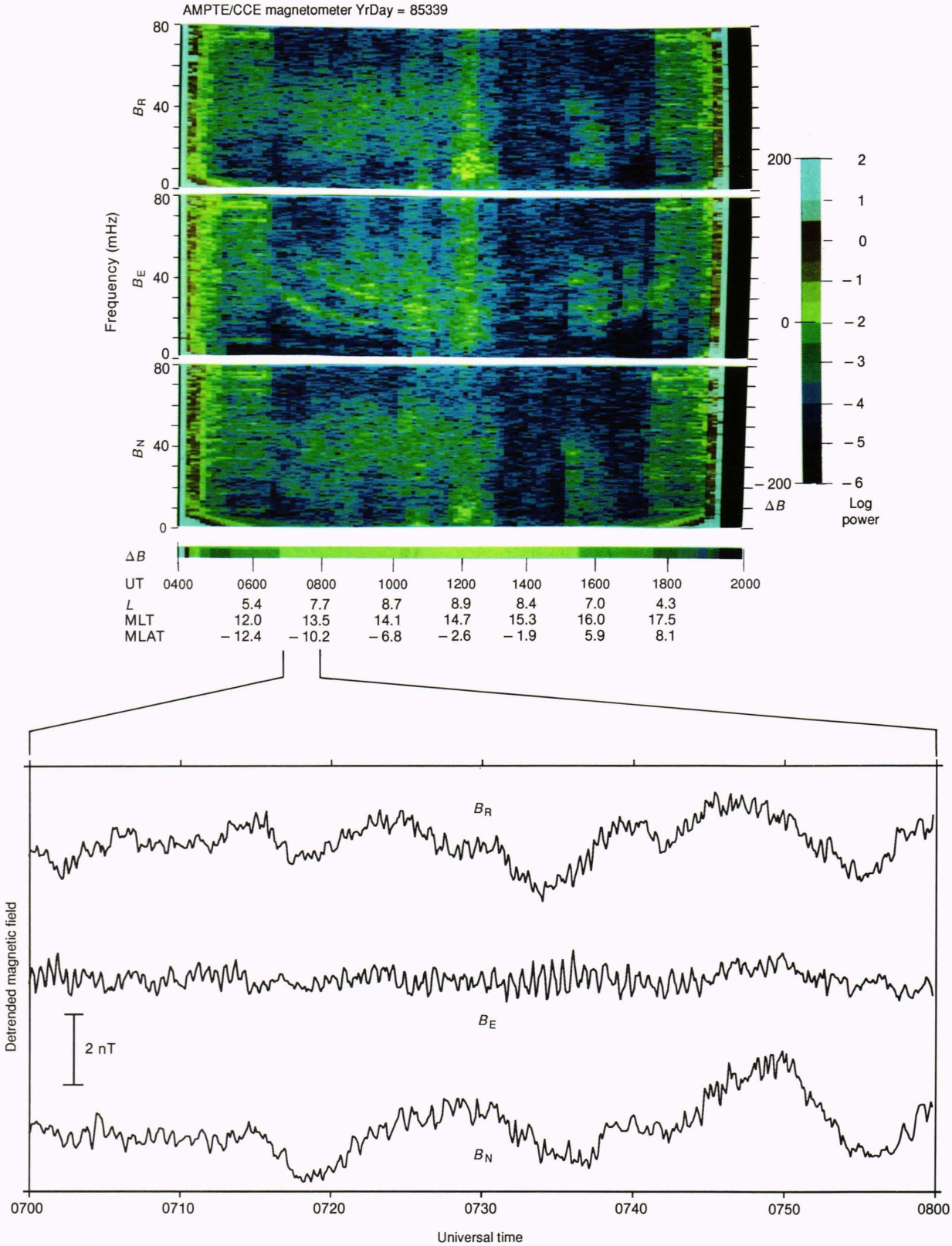

Figure 6. Harmonic toroidal mode field-line resonances observed by AMPTE/CCE in the same format as Figure 4. The detrended data (line plot) show that although the presence of azimuthal pulsations can be detected in line plots, the harmonic structure is virtually impossible to discern.

magnetic field and ion flux measurements that energetic ions are in bounce resonance with this type of wave, suggesting that the energetic ions are indeed the energy source for the wave.

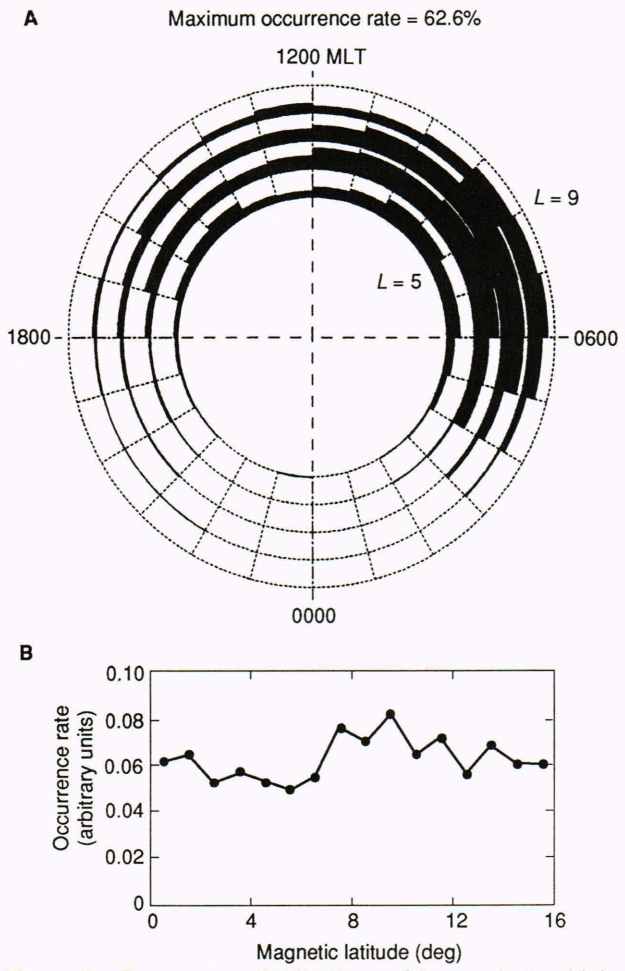

Figure 7. Occurrence distributions of harmonic toroidal mode resonances in the same format as Figure 5.

The fundamental toroidal, harmonic toroidal, and poloidal (second harmonic) modes are the three dominant classes of field-line resonances observed in the near equatorial magnetosphere, and their occurrence distributions suggest that three separate energy sources are responsible for them. Fundamental and harmonic resonances appear to be excited by a mechanism associated directly with the solar wind/magnetosphere interaction, whereas the poloidal second harmonic waves appear to be driven by ions in the magnetosphere.

PLASMA INSTABILITIES

Field-line resonances are a property of the magnetic field geometry, and their excitation reflects the distribution of energy sources whose frequencies and spatial structures match the frequency and spatial structure of the field-line perturbations. Two other types of pulsations occur commonly in the magnetosphere and result from instabilities in the magnetospheric ion population rather than from frequency matching to field lines. These additional pulsations are storm-time compressional waves with periods of 2 to 10 min, and electromagnetic ion cyclotron waves with frequencies of 0.1 to 4 Hz.

Storm-Time Compressional Waves

Storm-time compressional waves derive their name from their tendency to occur during geomagnetic storms, as observed at geostationary orbit. The reason for this association is that the ion populations required to excite the waves are energized and transported to geostationary distances during periods of high geomagnetic activity. An example of a storm-time compressional wave is shown in Figure 10. The pulsation occurs from 0000 to 0500 UT, and the wave has a large compressional, B_N, component. The latitude and L/MLT distributions of these waves are shown in Figure 11. A maximum occurrence at dusk and late evening at large L and confinement near the equator are evident. The prominence of activity on the nightside and to the west of midnight strongly suggests that ion populations injected from the nightside are responsible for the waves (recall that ions drift westward), consistent with their association with magnetic storms.

A rough idea of the physics behind these waves can be obtained by considering the interplay between particle magnetization currents and field inhomogeneity. Recall that the total pressure of the plasma is $P_{part} + B^2/2\mu_0$, and that the particle pressure can be written as $P_{part} = P_\perp + P_\parallel$. The perpendicular pressure provides a magnetic moment per unit volume of $\mathbf{m} = -P_\perp \mathbf{B}/B^2$, reflecting the diamagnetic nature of the plasma, and is associated with magnetization currents circulating in the left-hand sense. Note that $\mathbf{m}$ is inversely proportional to the field strength. A spatially uniform plasma in a uniform field is stable, but spatial inhomogeneities in the plasma density and field strength can lead to instabilities of spatial irregularities in the plasma density.[24]

Consider what happens when a cloud of high-$P_\perp$ plasma is injected into an inhomogeneous magnetic field, as illustrated in Figure 12. The boundary of the high-$P_\perp$ region is assumed to have a slight ripple structure, and the magnetic field increases to the right in the figure. Because the plasma magnetic moment is largest in the lower field regions, the associated magnetization currents are most intense in the portions of the ripple extending into the low field region and weaker along the valleys of the ripple. Because the magnetization currents are inhomogeneous, charge imbalance occurs, creating electric fields. The plasma responds to the electric field by drifting with a velocity $\mathbf{E} \times \mathbf{B}/B^2$, causing the rippled structure to grow larger, providing positive feedback. Gradients in the magnetic field and plasma density also cause drift motions of the plasma perpendicular to the gradients, so that the ripple structure moves parallel to the boundary of the high-$P_\perp$ region, creating a traveling wave. A common feature of these waves is that the magnetic field intensity and ion flux oscillate out of phase, consistent with this picture.[25]

Ion Cyclotron Waves

The second type of plasma wave with which we are concerned is associated with the ion cyclotron instability. This wave is also driven by an ion population with large $P_\perp$, but rather than being a pressure instability, the wave is generated by the cyclotron motion of the ions. Consider

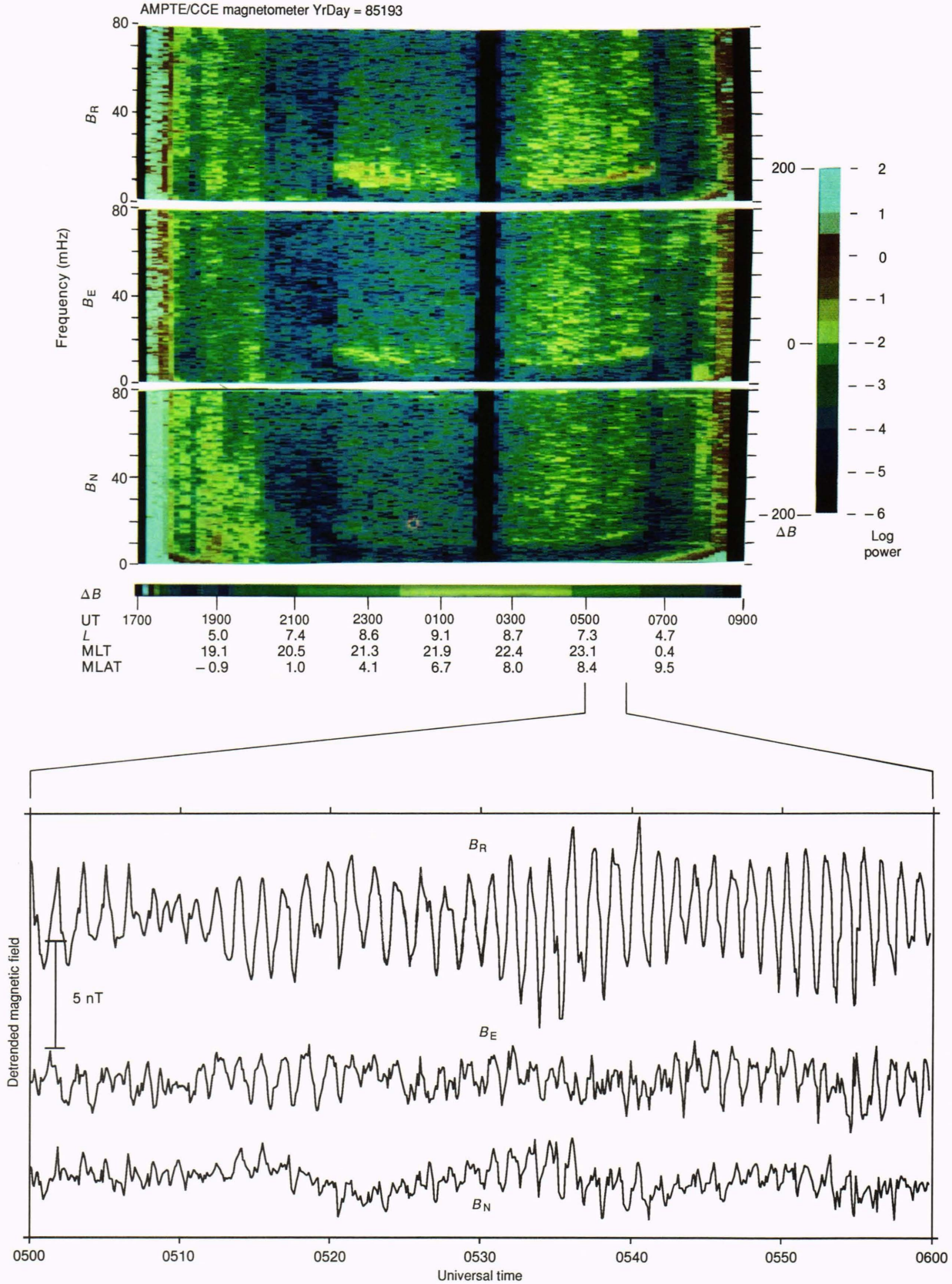

Figure 8. Poloidal mode field-line resonances observed by AMPTE/CCE in the same format as Figure 4. The dominance of the radial component is apparent in the waveform.

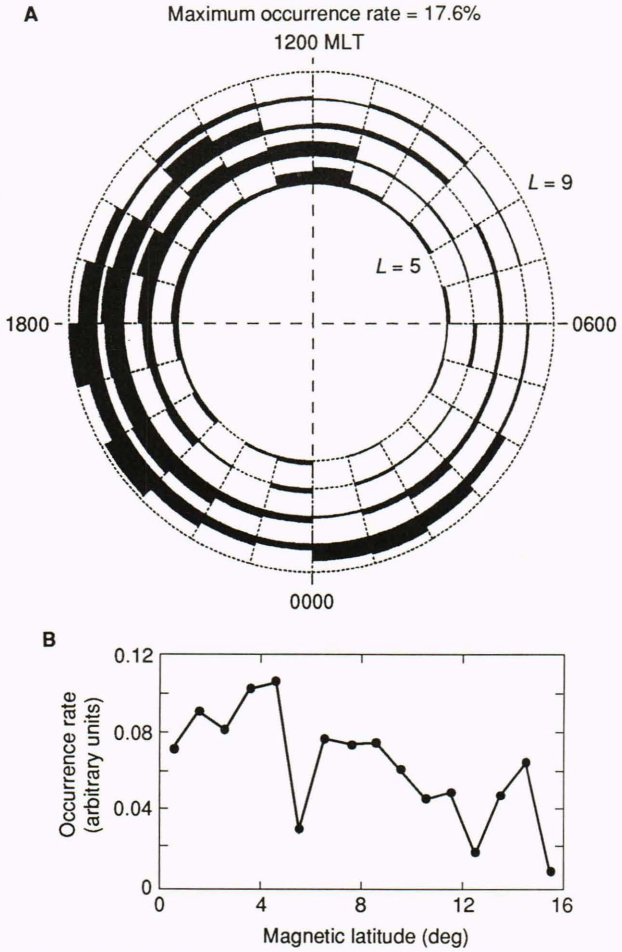

Figure 9. Occurrence distributions of poloidal mode resonances in the same format as Figure 5.

a particle with a velocity along the field line of $\mathbf{V}_\parallel$. An Alfvén wave propagating parallel to the field can interact resonantly with the particle if the matching condition $\omega = \Omega_c - \mathbf{k} \cdot \mathbf{V}_\parallel$ is met, that is, if the wave as viewed in the particle frame has the frequency Ω_c, the angular cyclotron frequency introduced earlier. Because ions gyrate in the left-hand sense, left-hand waves will be excited. To determine the frequencies that are unstable to growth, one must turn to the plasma dispersion relation, $D(\omega, \mathbf{k}) = 0$, and solve for $\omega(\mathbf{k}) = \omega_r + i\omega_i$, where ω_r and ω_i are the real and imaginary parts of the angular frequency, respectively. Determining the $\mathbf{k}$ for which ω_i is the largest positive value gives the growth rate versus ω_r. Results of these calculations show that growth occurs for $0.1\Omega_{H^+} < \omega < \Omega_{H^+}$, where Ω_{H^+} is the proton angular cyclotron frequency. The maximum frequency is determined by $P_\perp/P_\parallel$; larger $P_\perp/P_\parallel$ gives growth closer to Ω_{H^+}. The calculations also show that the presence of He^+ inhibits wave growth in the vicinity of the helium angular gyrofrequency, Ω_{He^+}.[26,27]

An example of electromagnetic ion cyclotron waves observed by AMPTE/CCE is shown in Figure 13. The top three panels in the spectrogram show the wave ellipticity in the plane perpendicular to **B**, the wave power transverse to **B**, and the wave power parallel to **B**. In the second and third panels, the dotted lines show the He^+ and H^+ cyclotron frequencies, respectively. The bottom panel shows energetic particle data from the Medium-Energy Particle Analyzer instrument. Waves occur from 0700 to 0930 UT for $L > 8$ and also at 0200 and 1445 UT at low L. For the $L > 8$ waves, onset occurs simultaneously with an enhancement in the energetic particle fluxes, indicating that the particles are intimately related to the waves. The wave occurs above the He^+ cyclotron frequency and is predominantly left-hand polarized. The L/MLT distribution of these waves (Fig. 14) shows a clear preference for occurrence in the early afternoon for $L > 7$ and a secondary population for $L > 8$ in the morning (0300–1000 MLT). The association with enhanced fluxes of $\approx$100-keV ions and theoretical expectations lead us to associate these waves with energetic ions. The high occurrence rate implies a significant energy transport out of the ion population into waves and eventually into the ionosphere.

ENERGY FLOW

These results have implications for the role of pulsations in energy flow in the magnetosphere. The pulsations discussed here all ultimately derive their energy from the interaction between the solar wind and the magnetosphere, and the energy delivered to the pulsations is eventually dissipated in the ionosphere. Magnetospheric pulsations therefore constitute a stage in the energy flow from the solar wind to the ionosphere, and the various pulsations can be viewed in terms of their position in an energy cascade. Possible energy pathways for the pulsations discussed here are shown schematically in Figure 15. The five classes of pulsations discussed earlier derive their energy from different mechanisms, but all of the mechanisms correspond to only two basic energy pathways: (1) direct excitation from the solar wind/magnetosphere interaction, and (2) instabilities driven by ion distributions that, in turn, result from acceleration processes occurring in the anti-sunward portion, or tail, of the magnetosphere.

Direct Conversion from the Solar Wind

Some energy from the solar wind appears to be converted directly into pulsations, namely, harmonic and fundamental toroidal mode resonances. Because these resonances appear to be driven by different interactions, at least two pathways must exist for channeling solar wind energy directly into pulsations. Two conventional mechanisms are (1) propagation of compressional wave power across the magnetopause and throughout the dayside magnetosphere, and (2) the Kelvin–Helmholtz (or wind-on-water) instability between shear plasma flows at the magnetopause and/or boundary layer regions just inside the magnetopause. These mechanisms are both shown schematically in Figure 15. In addition, evidence suggests that modulated ionospheric precipitation is associated with harmonic resonances. Turbulence just outside the magnetosphere may lead to modulated dayside ionospheric particle precipitation and hence conductivities and currents that could drive toroidal harmonic pulsations.[28]

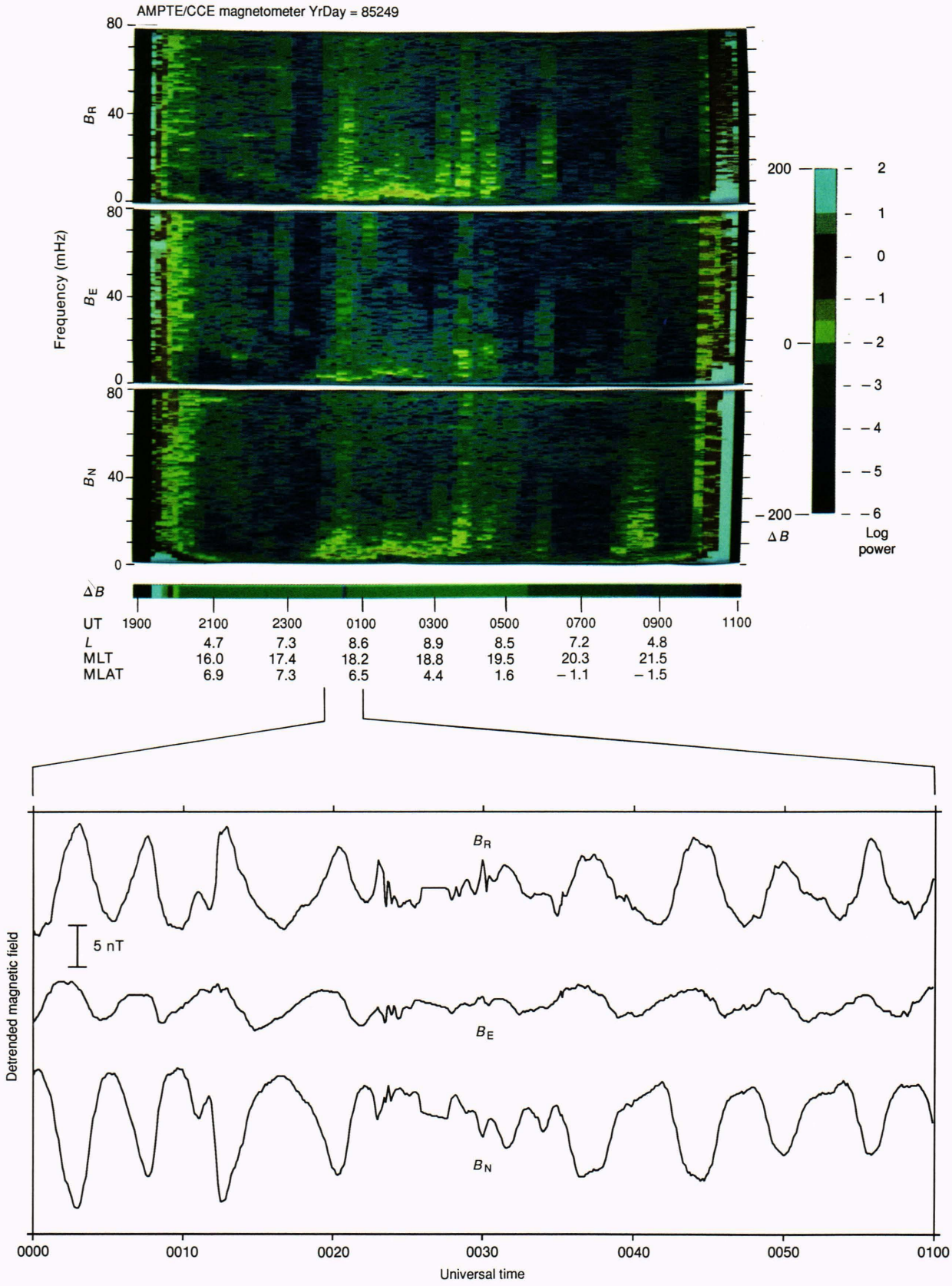

Figure 10. Storm-time compressional pulsations observed by AMPTE/CCE in the same format as Figure 4. The amplitude of the compressional component is large in contrast to the previous examples in which the compressional component was not appreciable.

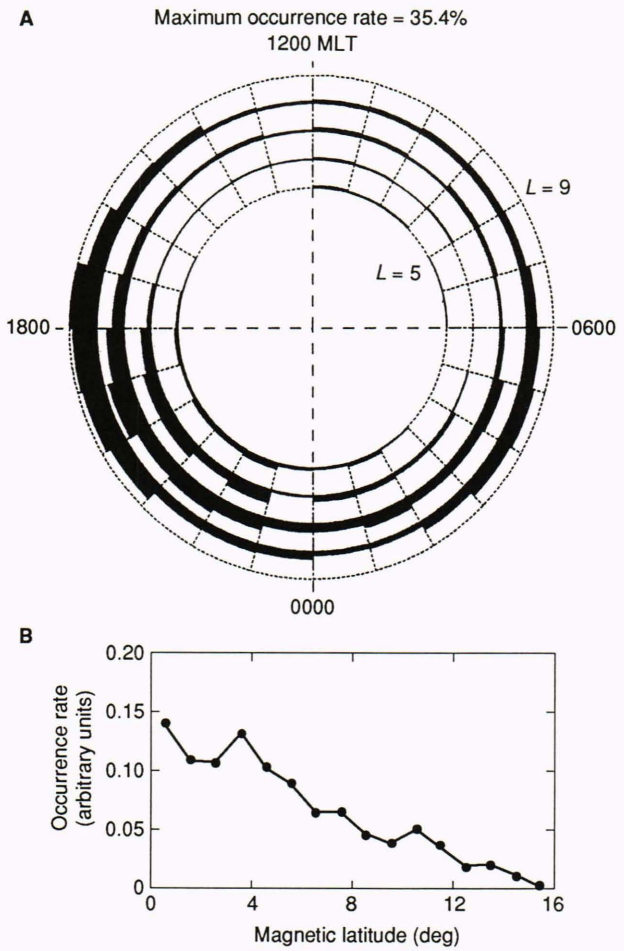

Figure 11. Occurrence distributions of storm-time compressional wave resonances in the same format as Figure 5.

Excitation due to Magnetospheric Ions

Many pulsations are driven by magnetospheric ion distributions. Ions energized in the magnetotail drift sunward under the influence of the dawn/dusk electric field, and close to the Earth they experience westward gradient curvature drift that diverts most of the ions to the dusk side of the magnetosphere. This drift pattern is illustrated in Figure 15. Poloidal second harmonic field-line resonances, storm-time compressional waves, and electromagnetic ion cyclotron waves all depend on magnetospheric ions for their energy, and all of these waves occur primarily on the dusk side. Because the spatial distributions of these waves are different, however, the ion distributions responsible for each type must also be different. Previous work has shown that storm-time compressional waves correlate with periods of geomagnetic activity, but the precise mechanisms responsible for producing the particle distributions responsible for each type of pulsation have not yet been identified. Nonetheless, for each of these pulsations, the energy conversion sequence is as follows: The solar wind/magnetosphere interaction generates electric fields, and the fields energize magnetospheric ions, which in turn excite geomagnetic pulsations.

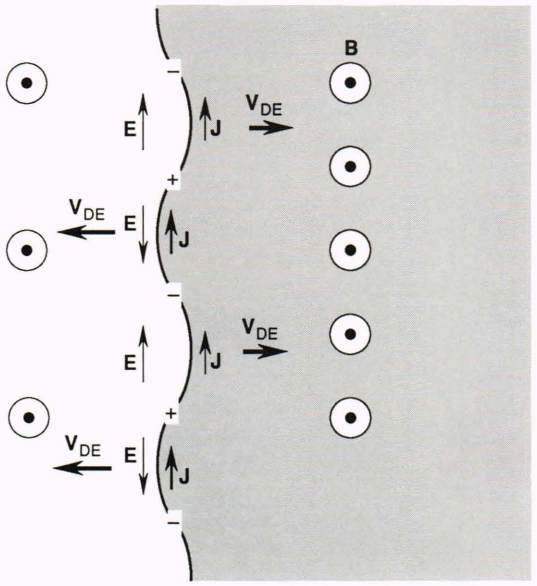

Figure 12. Illustration of the instability to wave growth of high-perpendicular-pressure plasma in an inhomogeneous magnetic field. The ripple corresponds to inhomogeneous magnetization currents that cause charge imbalance and hence electric fields. The electric fields cause plasma drift motions, making the ripple grow larger. In the figure, **B** is the magnetic field, **E** is the electric field, **J** is the current density, and $\mathbf{V}_{DE}$ is the plasma drift velocity.

Energy Budget

In terms of the overall magnetospheric energy budget, the majority of solar wind energy entering the magnetosphere is converted into ionospheric currents and particle precipitation in the auroral zone and amounts to a total power of roughly 10^{11} W. The power converted directly into pulsations is expected to be about 1% of this value. The existence of multiple pathways for energy input into pulsations may increase this percentage, however. In addition, pulsations deposit energy into the ionosphere equatorward of the auroral zone, so they will be relatively more important in these regions. It also appears that pulsations are one of the means by which ions that are accelerated during magnetically active periods convert their energy into forms that are deposited in the ionosphere. After a major magnetic storm, the energy content of energetic ions in the Earth's equatorial magnetosphere can be considerable (10^{15} J), so mechanisms for diverting some of this energy into the ionosphere may provide an appreciable source of energy.

Determining more precisely how the different types of pulsations are driven in the magnetosphere is a major objective of future pulsation research. As progress is made in this area, the role of pulsations in magnetosphere/ionosphere energy flow will be evaluated quantitatively.

REFERENCES

[1] Orr, D., "Magnetic Pulsations within the Magnetosphere: A Review," *J. Atmos. Terr. Phys.* **35**, 1–50 (1973).

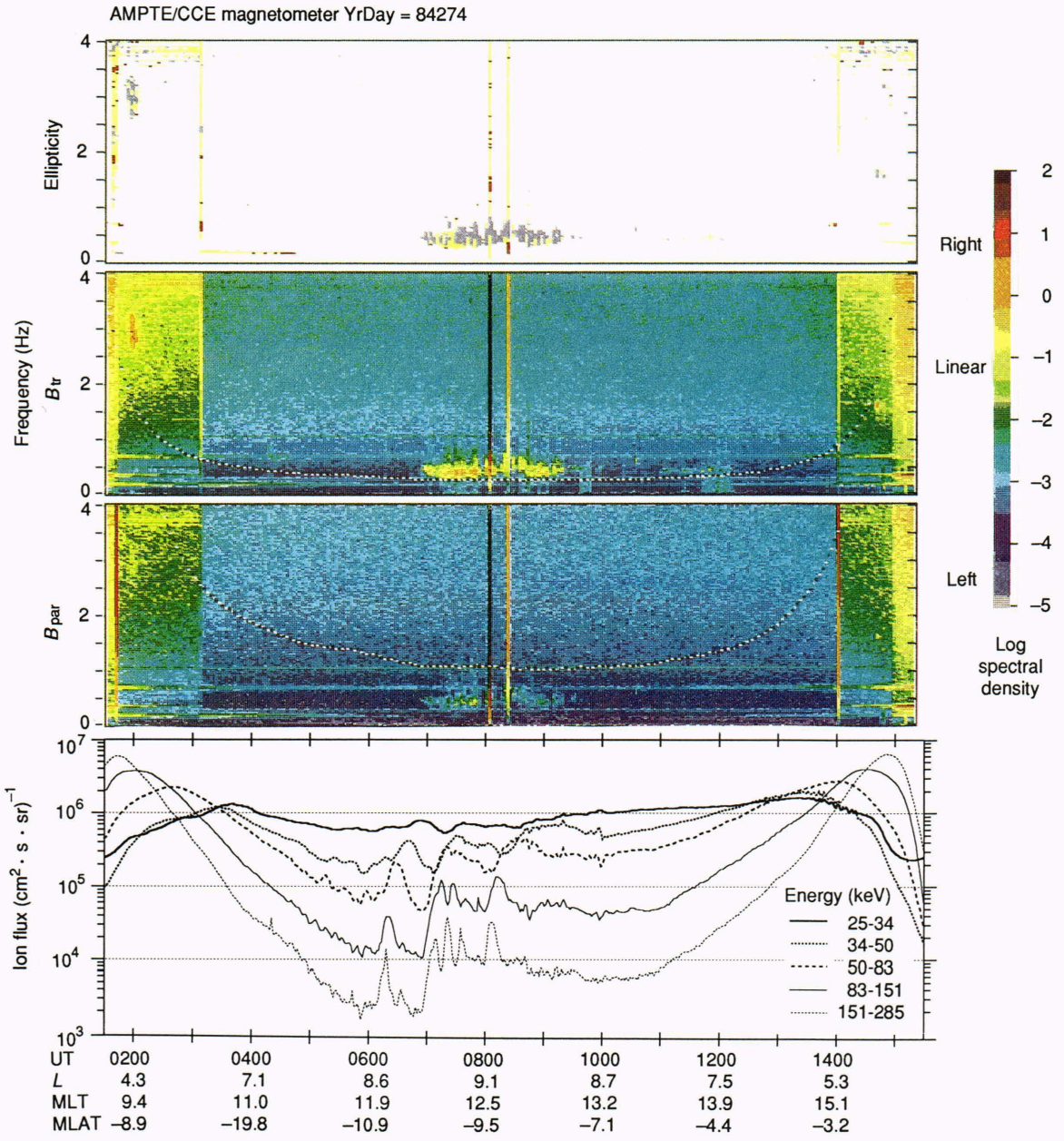

Figure 13. Electromagnetic ion cyclotron waves observed by AMPTE/CCE. The top three panels in the spectrogram show the wave ellipticity in the plane perpendicular to **B**, the wave power transverse to **B**, and the wave power parallel to **B**, respectively, for one satellite orbit. In the second and third panels, the dotted lines show the He^+ and H^+ cyclotron frequencies, respectively. The bottom panel shows energetic ion fluxes from the Medium-Energy Particle Analyzer instrument. Waves occur at 0200 UT, from 0700 to 0930 UT, and at 1445 UT, and are transverse (B_{tr}) and left-hand polarized (purple in the ellipticity panel). The onset of waves at 0700 UT occurs simultaneously with order of magnitude enhancements in >50 keV ion fluxes.

[2] Cahill, L. J., Jr., Lin, N. G., Engebretson, M. J., Weimer, D. R., and Sugiura, M., "Electric and Magnetic Observations of the Structure of Standing Waves in the Magnetosphere," *J. Geophys. Res.* **91**, 8895–8907 (1986).

[3] Takahashi, K., McEntire, R. W., Lui, A. T. Y., and Potemra, T. A., "Ion Flux Oscillations Associated with a Radially Polarized Transverse Pc 5 Magnetic Pulsation," *J. Geophys. Res.* **95**, 3717–3731 (1990).

[4] Hughes, W. J., "Multisatellite Observations of Geomagnetic Pulsations," *J. Geomagn. Geoelectr.* **32**, Suppl. II, SII 41–SII 55 (1980).

[5] Takahashi, K., "Multisatellite Studies of ULF Waves," *Adv. Space Res.* **8**, 427–436 (1988).

[6] Kokubun, S., "Observations of Pc Pulsations in the Magnetosphere: Satellite-Ground Correlation," *J. Geomagn. Geoelectr.* **32**, Suppl. II, SII 1–SII 15 (1980).

[7] Bryant, D. A., Krimigis, S. M., and Haerendel, G., "Outline of the Active Magnetospheric Particle Tracer Explorers (AMPTE) Mission," *IEEE Trans. Geosci. Remote Sensing* **GE-23**, 177–181 (1985).

[8] Potemra, T. A., Zanetti, L. J., and Acuña, M. H., "The AMPTE CCE Magnetic Field Experiment," *IEEE Trans. Geosci. Remote Sensing* **GE-23**, 246–249 (1985).

[9] Engebretson, M. J., Zanetti, L. J., Potemra, T. A., and Acuña, M. H., "Harmonically Structured ULF Pulsations Observed by the AMPTE CCE Magnetic Field Experiment," *Geophys. Res. Lett.* **13**, 905–908 (1986).

[10] Engebretson, M. J., Zanetti, L. J., Potemra, T. A., Klumpar, D. M., Strangeway, R. J., et al., "Observations of Intense ULF Pulsation Activity near the Geomagnetic Equator during Quiet Times," *J. Geophys. Res.* **93**, 12,795–12,816 (1988).

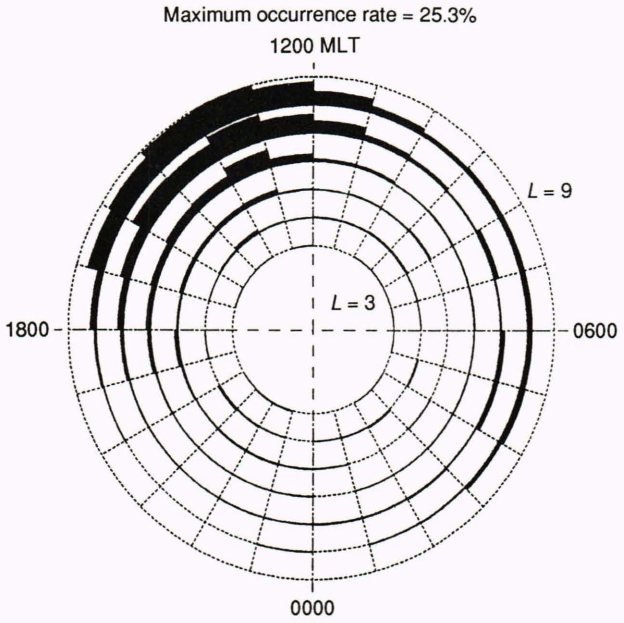

Figure 14. Equatorial occurrence distribution of electromagnetic ion cyclotron waves near the equator of the Earth's magnetosphere. The occurrence rate does not vary with latitude over the range ±16°. MLT is magnetic local time, and L is the equatorial crossing distance of the field line passing through the spacecraft in units of R_E.

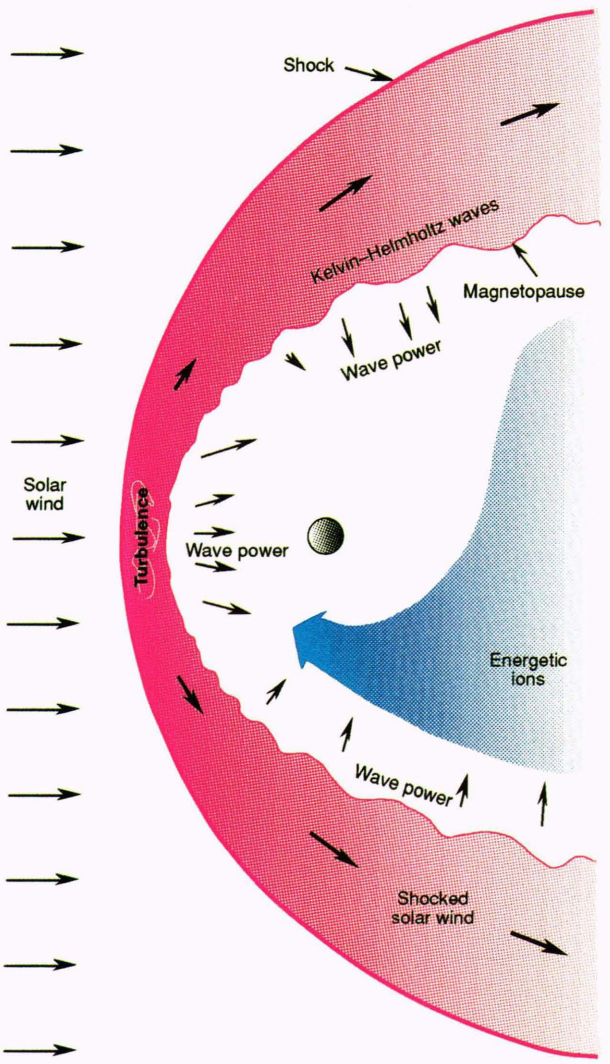

Figure 15. Diagram of energy sources and conversion pathways to geomagnetic pulsations. The solar wind flow is supersonic and develops a shock upstream of the magnetosphere. Energy is coupled to pulsations via several mechanisms: wave power is generated by turbulence outside the magnetosphere near noon and by Kelvin–Helmholtz waves at the magnetosphere flanks caused by velocity flow shear. This wave power propagates inward and couples to toroidal field-line resonances. Ions energized in the nightside magnetosphere are injected during magnetic activity and drift westward, through the late evening and dusk, providing energy for poloidal field-line resonances, storm-time compressional waves, and electromagnetic ion cyclotron waves.

[11] Takahashi, K., Cheng, C. Z., McEntire, R. W., Potemra, T. A., and Kistler, L. M., "Observation and Theory of Compressional Pc 5 Waves with a Second Harmonic Component," *J. Geophys. Res.* **95**, 977–989 (1990).

[12] Swanson, D. G., *Plasma Waves*, Academic Press, San Diego, Calif. (1989).

[13] Brice, N., "Fundamentals of Very Low Frequency Emission Generation Mechanisms," *J. Geophys. Res.* **69**, 4515–4522 (1964).

[14] Alfvén, H., *Cosmical Electrodynamics*, Oxford University Press, New York (1950).

[15] Cummings, W. D., O'Sullivan, R. J., and Coleman, P. J., Jr., "Standing Alfvén Waves in the Magnetosphere," *J. Geophys. Res.* **74**, 778–793 (1969).

[16] Lee, D.-L., and Lysak, R. L., "Magnetospheric ULF Wave Coupling in the Dipole Model: The Impulsive Excitation," *J. Geophys. Res.* **94**, 17,097–17,103 (1989).

[17] Chen, L., and Hasegawa, A., "A Theory of Long-Period Magnetic Pulsations: 1. Steady State Excitation of Field Line Resonances," *J. Geophys. Res.* **79**, 1024–1032 (1974).

[18] Chen, L., and Crowley, S. C., "On Field Line Resonances of Hydromagnetic Alfvén Waves in Dipole Magnetic Field," *Geophys. Res. Lett.* **16**, 895–897 (1989).

[19] Anderson, B. J., Engebretson, M. J., Rounds, S. P., Zanetti, L. J., and Potemra, T. A., "A Statistical Study of Pc 3–5 Pulsations Observed by the AMPTE/CCE Magnetic Fields Experiment. 1. Occurrence Distributions," *J. Geophys. Res.* **95**, 10,495–10,523 (1990).

[20] Kivelson, M. G., and Pu, Z.-Y., "The Kelvin–Helmholtz Instability on the Magnetopause," *Planet. Space Sci.* **32**, 1335–1341 (1984).

[21] Takahashi, K. T., McPherron, R. L., and Terasawa, T., "Dependence on the Spectrum of Pc 3–4 Pulsations on the Interplanetary Magnetic Field," *J. Geophys. Res.* **89**, 2770–2780 (1984).

[22] Engebretson, M. J., Zanetti, L. J., Potemra, T. A., Baumjohann, W., Lühr, H., et al., "Simultaneous Observation of Pc 3–4 Pulsations in the Solar Wind and in the Earth's Magnetosphere," *J. Geophys. Res.* **92**, 10,053–10,062 (1987).

[23] Hughes, W. J., Southwood, D. J., Mauk, B., McPherron, R. L., and Barfield, J. N., "Alfvén Waves Generated by an Inverted Plasma Energy Distribution," *Nature* **275**, 43–45 (1978).

[24] Miura, A., Ohtani, S., and Tamao, T., "Ballooning Instability and Structure of Diamagnetic Hydromagnetic Waves in a Model Magnetosphere," *J. Geophys. Res.* **94**, 15,231–15,242 (1989).

[25] Kremser, G., Korth, A., Fejer, J. A., Wilken, B., Gurevich, A. V., et al., "Observations of Quasi-Periodic Flux Variations of Energetic Ions and Electrons Associated with Pc 5 Geomagnetic Pulsations," *J. Geophys. Res.* **86**, 3345–3356 (1981).

[26] Gomberoff, L., and Cuperman, S., "Combined Effect of Cold H^+ and He^+ Ions on the Proton Cyclotron Electromagnetic Instability," *J. Geophys. Res.* **87**, 95–100 (1982).

[27] Gomberoff, L., and Niera, R., "Convective Growth Rate of Ion Cyclotron Waves in a H^+–He^+ and H^+–He^+–O^+ Plasma," *J. Geophys. Res.* **88**, 2170–2174 (1983).

[28] Engebretson, M. J., Anderson, B. J., Cahill, L. J., Jr., Arnoldy, R. L., Rosenberg, T. J., et al., "Ionospheric Signatures of Cusp Latitude Pc 3 Pulsations," *J. Geophys. Res.* **95**, 2447–2456 (1990).

ACKNOWLEDGMENTS: Analysis of AMPTE/CCE magnetic field data was supported by NASA, by the National Science Foundation (NSF), and by the Office of Naval Research. Support for computational work completed at Augsburg College was provided by NSF.

THE AUTHOR

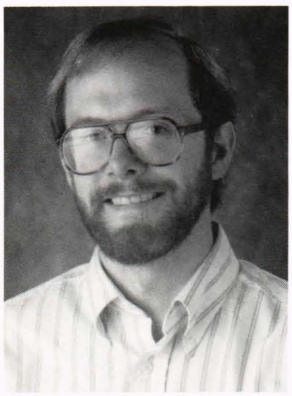

BRIAN J. ANDERSON was born in Minneapolis, Minnesota, in 1959. He obtained a B.A. in physics from Augsburg College, Minneapolis, Minnesota, in 1982 and a Ph.D. in physics, specializing in experimental mass spectroscopy, from the University of Minnesota in 1987. He returned to Augsburg College as an Assistant Professor of Physics, where he began his research on magnetospheric pulsations. He came to APL's Space Department in 1988 as a Postdoctoral Associate.